AFRL-RW-EG-TR-2014-135

Physiochemical Characterization of Iodine (V) Oxide: Hydration Rates

Brian K. Little
Samuel B. Emery
Joshua C. Nittinger
Ryan C. Fantasia
C. Michael Lindsay

Air Force Research Laboratory
Munitions Directorate/Ordnance Division
Energetic Materials Branch (AFRL/RWME)
Eglin AFB, FL 32542-5910

December 2014

Final Report

AIR FORCE RESEARCH LABORATORY, MUNITIONS DIRECTORATE

Air Force Materiel Command ■ United States Air Force ■ Eglin Air Force Base

NOTICE AND SIGNATURE PAGE

Using Government drawings, specifications, or other data included in this document for any purpose other than Government procurement does not in any way obligate the U.S. Government. The fact that the Government formulated or supplied the drawings, specifications, or other data does not license the holder or any other person or corporation; or convey any rights or permission to manufacture, use, or sell any patented invention that may relate to them.

Qualified requestors may obtain copies of this report from the Defense Technical Information Center (DTIC) (http://www.dtic.mil).

AFRL-RW-EG-TR-2014-135 HAS BEEN REVIEWED AND IS APPROVED FOR PUBLICATION IN ACCORDANCE WITH ASSIGNED DISTRIBUTION STATEMENT.

FOR THE DIRECTOR:

WHITE.HOWARD.G.1230779062
Digitally signed by WHITE.HOWARD.G.1230779062
DN: c=US, o=U.S. Government, ou=DoD, ou=PKI, ou=USAF, cn=WHITE.HOWARD.G.1230779062
Date: 2014.12.15 07:49:44 -06'00'

HOWARD G. WHITE, PhD
Chief Engineer
Ordnance Division

Digitally signed by LINDSAY.C.MICHAEL.1282886614
DN: c=US, o=U.S. Government, ou=DoD, ou=PKI, ou=USAF, cn=LINDSAY.C.MICHAEL.1282886614
Date: 2014.12.15 07:18:46 -06'00'

C. MICHAEL LINDSAY, PhD
Technical Advisor
Energetic Materials Branch

BOGLE.MITCHELL.B.1185859068
Digitally signed by BOGLE.MITCHELL.B.1185859068
DN: c=US, o=U.S. Government, ou=DoD, ou=PKI, ou=USAF, cn=BOGLE.MITCHELL.B.1185859068
Date: 2014.12.12 14:55:07 -06'00'

MITCHELL B. BOGLE
Program Manager
Energetic Materials Branch

This report is published in the interest of scientific and technical information exchange, and its publication does not constitute the Government's approval or disapproval of its ideas or findings.

This page intentionally left blank

REPORT DOCUMENTATION PAGE

Form Approved
OMB No. 0704-0188

1. REPORT DATE *(DD-MM-YYYY)*	**2. REPORT TYPE**	**3. DATES COVERED** *(From - To)*
15 – 12- 2014	Final	October 2011 – August 2014

4. TITLE AND SUBTITLE

Physiochemical Characterization of Iodine (V) Oxide: Hydration Rates

5a. CONTRACT NUMBER

5b. GRANT NUMBER

5c. PROGRAM ELEMENT NUMBER
62602F

6. AUTHOR(S)
Brian K. Little, Samuel B. Emery, Joshua C. Nittinger, Ryan C. Fantasia and C. Michael Lindsay

5d. PROJECT NUMBER
25029946

5e. TASK NUMBER

5f. WORK UNIT NUMBER
W0DC

7. PERFORMING ORGANIZATION NAME(S) AND ADDRESS(ES)

Air Force Research Laboratory, Munitions Directorate
Ordnance Division
Energetic Materials Branch (AFRL/RWME)
Eglin AFB FL 32542-5910

8. PERFORMING ORGANIZATION REPORT NUMBER

AFRL-RW-EG-TR-2014-135

9. SPONSORING / MONITORING AGENCY NAME(S) AND ADDRESS(ES)

Air Force Research Laboratory, Munitions Directorate
Ordnance Division
Energetic Materials Branch (AFRL/RWME)
Eglin AFB FL 32542-5910
Technical Advisor: C. Michael Lindsay, PhD

10. SPONSOR/MONITOR'S ACRONYM(S)
AFRL/RWME

11. SPONSOR/MONITOR'S REPORT NUMBER(S)
AFRL-RW-EG-TR-2014-135

12. DISTRIBUTION / AVAILABILITY STATEMENT

Distribution A: Approved for public release; distribution unlimited. Approval Confirmation 96 ABW/-2014-0078, dated 21 March 2014

13. SUPPLEMENTARY NOTES **SUBJECT TO EXPORT CONTROL LAWS**
DISTRIBUTION STATEMENT INDICATING AUTHORIZED ACCESS IS ON THE COVER PAGE AND BLOCK 12 OF THIS FORM.
DATA RIGHTS RESTRICTIONS AND AVAILABILITY OF THIS REPORT ARE SHOWN ON THE NOTICE AND SIGNATURE PAGE.

14. ABSTRACT

In the first of a series of papers on the iodine (V) oxide system, the chemical and physical properties associated with iodine (V) oxide in its anhydride (I_2O_5) and hydrated states (HI_3O_8 and HIO_3) are examined. The three forms of the oxide have been investigated utilizing differential scanning calorimetry (DSC), thermogravimetric analysis (TGA), and powder X-ray diffraction (PXRD). In addition, the hydration rates governing the conversion of the anhydride (I_2O_5) to the initial hydrate (HI_3O_8) and later to the final hydrated state (HIO_3) are reported and discussed. Results from this study suggest that the hydration mechanism for $I_2O_5 \rightarrow HI_3O_8$ begins with an accelerating period described as a nucleation and growth phase followed by a decelerating period that is diffusion limited. The initial rate of hydration was observed to be governed by the nucleation and growth mechanism, which was inhibited by covering the surface of the particle with an inert metal. Based on this investigation the initial rate of hydration appears to be strongly dependent on the anhydride's available surface area which facilitates nucleation and growth of HI_3O_8.

15. SUBJECT TERMS
Iodine (V) oxide, iodine pentoxide, I_2O_5, hydrogen iodate, triperiodic acid, HI_3O_8, HIO_3-I_2O_5, iodic acid, HIO_3, energetic material, hydration rate, oxidizer

16. SECURITY CLASSIFICATION OF:			**17. LIMITATION OF ABSTRACT**	**18. NUMBER OF PAGES**	**19a. NAME OF RESPONSIBLE PERSON**
					Mitchell Bogle
a. REPORT	**b. ABSTRACT**	**c. THIS PAGE**			**19b. TELEPHONE NUMBER** *(include area code)*
UNCLASSIFIED	UNCLASSIFIED	UNCLASSIFIED	SAR	28	850-882-5600

Standard Form 298 (Rev. 8-98)
Prescribed by ANSI Std. Z39.18

This page intentionally left blank

TABLE OF CONTENTS

LIST OF FIGURES

1. INTRODUCTION

Metal-oxidizer systems (*e.g.* thermites) show promise as alternative energetic materials for explosive applications owing to their higher energy density and ability to vary their output between thermal and P-V work.[1,2] The primary limitation of such systems, however, has been rate of energy release. In monomolecular organic explosives (*e.g.* TNT, RDX, or CL-20) the fuel and oxidizer are located on the same molecule and thus have only a few Ångstroms to travel to react, whereas metaloxidizer systems are usually formed from mixed powders and have mass diffusion limitations characteristic of the particle size.[3] The rate of reaction can be increased by reducing the particle size, and several systems at the nanoscale have demonstrated >1 km/s combustion speeds.[4,5,6,7] Systems with the highest combustion speeds tend to contain oxidizers that generate gaseous products, and these include oxides of bismuth, iodine, and copper as well as fluorocarbons.[8]

In addition to the chemical composition, particle size, mixture homogeneity, and degree of gas evolution during the reaction, there are several other factors which are known to affect the reactivity of metal-oxidizer systems. Properties such as density, porosity, crystallinity, stability and morphology are known to impact initiation thresholds and detonation velocities in conventional explosives and can have similar effects in nonmonomolecular energetic systems.[9-14] Unlike metal fuels (Al, Cu, B, etc.) and metal oxides (CuO, Fe_2O_3, WO_3, etc.) which can be obtained at the nanoscale through commercial sources, halogen based oxidizers are typically purchased at the micron scale and then processed to smaller more uniform particle sizes. Also, in general, less is known about the purity and stability to hydration of these oxidizers in energetic blends as compared to metal/metal-oxide blends *e.g.* Al/Fe_2O_3. Thus, knowledge of the fundamental properties such as hydration stability per particle size, morphology, crystallinity and phase of the oxidizer is essential in unraveling the chemistry of energetic blends composed of a fuel and such oxidizer.

Of particular interest are iodine oxide based systems. The most promising iodine oxide composite is thought to be iodine pentoxide/nano-aluminum which has been shown to produce peak pressures as high as 11 GPa and combustion speeds of ~2000 m/s in loose powders.[7,8,15] These values are approaching those of traditional monomolecular explosives such as TNT which has a detonation pressure of 21 GPa and a detonation velocity of 6.7 km/s.[16] However, unlike monomolecular explosives whose main purpose is to drive a blast wave, metaloxidizer systems hold the potential to deliver a blast wave, a thermal wave, and in the case of the iodine oxides, a biocidal effect.[3,17,18]

This study is the first in a series aimed at examining the chemicophysical properties of the iodine (V) oxide system. Specifically, we identify the anhydrous and hydrated forms of the oxidizer and investigate the mechanism of hydration between them. This work utilizes DSC, TGA and PXRD measurements to provide a clear picture of the hydration mechanism of I_2O_5.

2. BACKGROUND

Iodine commonly takes on oxidation states ranging from -1 to +7 and its oxides are widely known.[19] The oxides of iodine in its +5 state include I_2O_5, HI_3O_8 (or more specifically, the HIO_3-I_2O_5 adduct), and HIO_3. Each was discovered in 1815 but were not confirmed confidently until 1968 when the compounds were synthesized and verified utilizing modern instrumentation.[20,21] Many analytical techniques have since been utilized to investigate this system including X-ray diffraction, infrared and Raman spectroscopy, mass spectroscopy, thermal gravimetric, differential scanning calorimetry, nuclear magnetic resonance(I^{151}, H^1), and X-ray photoelectron spectroscopy with most of this work conducted in the mid-20th century.[21,22,23,24,25] Although there is substantial information on I_2O_5 in the literature it is either incomplete or contradictory with respect to the structure and stability of this compound.[19,22,26,27] The lack of consistency in validating the structure of I_2O_5 is predominantly due to its hygroscopic nature, in that there is a strong propensity to form HI_3O_8 and the more thermodynamic favorable hydride, HIO_3 in the presence of excess water.[19,21,26] Matters are further compounded by the fact that the purity of most commercial products has been historically unreliable.[21,28] Consequently, the iodine oxide family as a whole is incompletely characterized, particularly with respect to their formation and decomposition pathways.[19]

I_2O_5 has been reportedly prepared in numerous ways but many of these reports have not held up to scrutiny.[19] The simplest methods for forming I_2O_5 is by either oxidizing iodine with fuming nitric acid at room temperature or through ozonization of dissolved iodine in anhydrous CCL_4.[29] Both methods were independently validated by Selte and Kjekhus.[21] Alternatively, I_2O_5 can be produced by thermally dehydrating HIO_3, HI_3O_8, H_5IO_6, or I_2O_4.[21,30]

In sufficiently humid environments, iodine (V) oxides undergo deliquescence (the absorption of so much water vapor that an aqueous solution is produced). Selte and Kjekshus reported observing a high degree of susceptibility to deliquescence for smaller particles on the order of a few microns.[21] Another study conducted by Kumar *et al.* reports the stability of micron particles of iodine oxides (I_2O_5 and HIO_3) as a function of relative humidity (RH).[31] They reported that I_2O_5 and HIO_3 undergo deliquescence at 80.8 ± 1% and 85.0 ± 1% relative humidity respectfully for micron size crystals (10-50 μm). The product material after evaporation of a delinquent solution is less clear, with both HI_3O_8 and HIO_3 being reported.[31] Scheme 1 details the generally accepted hydration/dehydration steps for iodine (V) oxide as well as its thermal decomposition.[21]

Scheme 1. Iodine (V) Oxide-Water System

Hydration:

$$3I_2O_5(s) + H_2O(g) \rightarrow 2HI_3O_8(s) + 2H_2O(g) \rightarrow 6HIO_3(s)$$

Dehydration:

$$6HIO_3(s) \rightarrow 2H_2O(g) + 2HI_3O_8(s) \rightarrow H_2O(g) + 3I_2O_5(s)$$

Decomposition:

$$I_2O_5(s) \rightarrow 3/2O_2(g) + I_2(g)$$

3. EXPERIMENTAL SECTION

3.1. Materials

I_2O_5 (advertised 98% purity, though it was found to be almost entirely HI_3O_8) was purchased from Acrōs Organics and is labeled throughout as sample "A". Sample "$A_{recrystalized}$" is "A" dissolved in deionized water, recrystallized through evaporation. It is important to note that when dissolved in water, I_2O_5, HI_3O_8, or HIO_3 can precipitate out in any of the three hydration forms (predominately as one form, but mixtures were observed occasionally) in contrast to Reference 21 which reports exclusively the formation of HIO_3. Which product one obtains depends sensitively on the presence of impurities, rate of evaporation, and crystal size upon precipitation and care must be taken to examine the composition of the resulting material. In order to facilitate hydration of HI_3O_8 into HIO_3 the precipitate was pulverized into fine particles and exposed to relative humidity (RH) above ~60%. Note: "as received" particles of HI_3O_8 can be hydrated without pulverization, *i.e.* coarser particles, as long as the RH is greater than 65%. Sample "$A_{recrystalized,hydrated}$" is sample "Arc" that has completely hydrated into to HIO_3.

In order to study the anhydrous form, I_2O_5 was generated by ball-milling commercial material under nitrogen and stored under dry argon.[2,6] This material is denoted as "B" and consists of particles <1 μm.

3.2. Analysis and Preparation

Thermal Gravimetric Analysis (TGA)/Differential Scanning Calorimetry (DSC): samples (10-30 mg) were measured with a Mettler-Toledo TGA/DSC Star System at a ramp rate of 2 °C/min under dry air using open or closed alumina crucibles; closed crucibles were contained with a lid that had a small pin hole. *Powdered X-ray Diffraction (PXRD)*: X-ray diffractograms (XRD patterns) were recorded between the scan range of 2θ = 8 and 80 degrees using a Cu radiation source (Cu Kα, λ = 1.54178 Å) on a Philips X'Pert Pro MPD diffractometer. Samples were

rotated on a stage during the analysis and prepared by centering the powder on a zero background holder. *Scanning Electron Microscopy (SEM)*: electron images were acquired using a JEOL JSM- 5900LV microscope. Samples were prepared by adhering the sample powder to carbon tape on an aluminum stub. All samples were sputter coated with a thin layer of Au/Pd (5-10 nm thick) to minimize the effects of charging.

3.3. Calculations

TGA: The composition of the various samples was determined by measuring the H_2O mass loss upon dehydration of HIO_3 and/or HI_3O_8 at 100 °C and 210 °C, respectively. This mass loss was related to % I_2O_5, HI_3O_8, and HIO_3 using the stoichiometry of the dehydration mechanism in Scheme 1.[21]

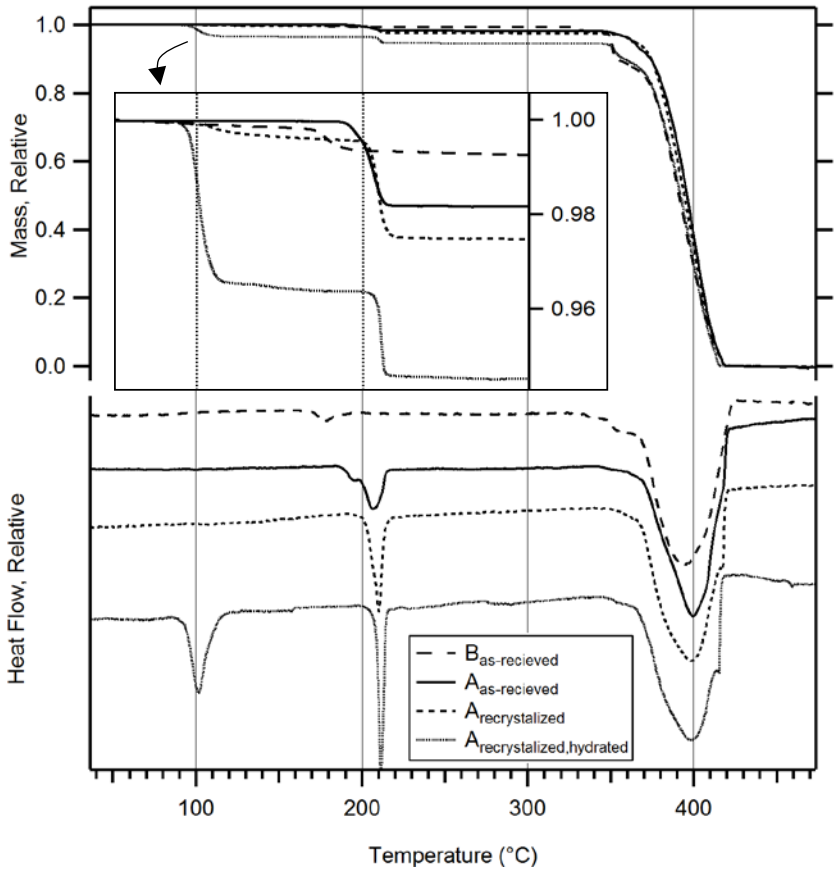

Figure 1. Plot of heat flow (bottom) and mass loss (top) in a sample as a function of temperature obtained by differential scanning calorimeter (DSC) and thermal gravimetric analysis (TGA) for sample set "A". The inset expands the vertical axis to show the details of the mass loss upon dehydration at 100 °C and 210 °C. Samples were run under air at a temperature ramp rate 2 °C/min.

PXRD:

The composition of the various samples was also determined by comparing the integrated areas of the strongest diffraction peak of I_2O_5, HI_3O_8, and HIO_3. These correspond to peak's with Miller Index of <210> for I_2O_5, <121> for HI_3O_8, and <110> for HIO_3 scattering at 2 theta = 24.4°, 27.2° and 22.0°, respectively. The fraction of each substance was calculated by dividing the integrated area of strongest peak, by the sum of the integrated areas of all of the strongest peaks. Each peak's intensity was scaled by the inherent reflection intensity as obtained from powder diffraction cards for I_2O_5 (04-007-1333)[22], HI_3O_8 (04-011- 9546)[23], and HIO_3 (04-010-6560)[24]:

$$\% I_2O_5 = 100 \times (I_{<210>}/4.69)/ (I_{<210>}/4.69 + I_{<121>}/3.47 + I_{<110>}/5.49)$$

$$\% HI_3O_8 = 100 \times (I_{<121>}/3.47)/ (I_{<210>}/4.69 + I_{<121>}/3.47 + I_{<110>}/5.49)$$

$$\% HIO_3 = 100 \times (I_{<110>}/5.49)/ (I_{<210>}/4.69 + I_{<121>}/3.47 + I_{<110>}/5.49)$$

4. RESULTS

4.1. Composition of the Original Samples

Figure 1 is a plot of the heat flow and mass loss thermograms from the DSC/TGA of sample "A", as received, upon recrystallization, and after being fully converted to HIO_3. Selte and Kjekshus first characterized the endotherms[21] of the iodine (V) oxide system via differential thermal analysis (DTA) and attributed the features at ~100 °C, ~210 °C, and ~400 °C to the dehydration of HIO_3 into the molecule HI_3O_8, the dehydration of HI_3O_8 into I_2O_5 and the melting/decomposition of I_2O_5 into O_2 and I_2, respectively. Immediately apparent from the DSC traces is that the as-received "I_2O_5," sample A, contains a large amount of HI_3O_8, as indicated by the pair of peaks near ~200 °C. The lower temperature peak at 195 °C is indicative of an amorphous phase of HI_3O_8 and generally occurs when I_2O_5 is hydrated into HI_3O_8 via humid air (see section 4.2 for further discussion). The combined mass loss of 1.770 % from the TGA indicates that 100% of the sample is HI_3O_8 and that none is I_2O_5. Great care was taken to protect the as-received material from incidental hydration in the air during the transfer of the material from the bottle in this measurement. As discussed in the background, the purity of the as-received commercial material historically has been problematic and indeed is the case with this particular supplier and lot.

Upon dissolving the as-received material in water and recrystallizing it through evaporation, *i.e.* sample "$A_{recrystalized}$", the sample produces a single, sharp endotherm and mass loss near at the 210 °C in the DSC/TGA. The lack of a mass loss/endotherm ~100 °C and the presence of the 210 °C features indicate that the iodine (V) oxide system precipitated out from the aqueous solution as HI_3O_8. Interestingly, when this precipitated material is exposed to humid air

(RH >65%), it hydrates to HIO_3, as evidenced by the appearance of the endotherm and mass loss at ~100 °C in the DSC/TGA data from samples "$A_{recrystalized,hydrated}$." To validate this assertion, a sample of pure HIO_3 was dissolved in water, evaporatively precipitated/recrystallized, and was confirmed to form pure HI_3O_8 in some of the samples (not shown). Once pulverized, and exposed to humid air with a RH greater than 65%, it indeed reformed HIO_3. This complex hydration process is likely due to a surface assisted vapor-solid interfacial mechanism, commonly referred to as a topochemical reaction, which is a known pathway for hydration mechanisms and is probably responsible for much of the confusion in material composition found in the literature and in commercially available products. It is important to note that upon multiple repetitions of this experiment (dissolving in water then precipitating out) over a period of weeks, the dry precipitate was sometimes found to be HIO_3, sometimes HI_3O_8, and on one rare, occasion, I_2O_5. The reason for this variability is likely due to the rate of water evaporation, presence of impurities, and possibly, presence of seed crystals.

A sample thought to contain mostly I_2O_5, sample "B," was also analyzed. Indeed, the mass loss attributed to dehydration of HI_3O_8 is much lower (0.45%) than those of the "A" samples, indicating that most of the materials are in the anhydrous form, I_2O_5. Interestingly, the peak associated with the small amount of dehydration is shifted to lower temperature (~180 °C), a subject that will be investigated more thoroughly below.

All of the samples in Figure 1 exhibit qualitatively identical behavior in the DSC/TGA data between 360 °C and 420 °C. The broad mass loss and endothermic features are attributed to the decomposition of I_2O_5 [21] and indicate that in all samples, regardless of the initial hydration state, completely dehydrate into I_2O_5 above ~ 220 °C. Table 1 summarizes the fractional mass loss observed for the two dehydration steps and decomposition step for each sample. The corresponding percent compositions of the three hydration forms of the oxide have been calculated from these TGA mass losses assuming the stoichiometry of Scheme 1. It is evident that there is a small amount of impurity (likely entrapped water) in the sample as there is a small amount of mass loss (<1%) observed in the thermograms without a corresponding endothermic peak.

Table 1. Composition of the various samples of "I_2O_5", as-received, recrystallized, and after hydration as determined from the TGA mass losses. Numbers in parenthesis are the uncertainty in the last digits of the measurement.

Sample	H_2O loss *T*~100 °C	H_2O loss *T*~210	I_2O_5 loss T~400 °C	HIO_3	HI_3O_8	I_2O_5
$A_{as\text{-}received}$	0.00(1)%	1.77(3)%	98.09(3)%	0.0%	100.2%	-0.2%
$A_{recrystalized}$	0.00(1)%	2.02(4)%	97.44(3)%	0.0%	114.4%	-14.4%
$A_{recrystalized,\ hydrated}$	3.42(2)%	1.77(4)%	94.40(15)%	100.3%	3.4%	-3.6%
$B_{as\text{-}recieved}$	0.00(1)%	0.45(4)%	99.29(5)%	0.0%	25.5%	74.5%

PXRD spectra of samples "$A_{as\text{-}received}$", "$A_{recrystalized,hydrated}$" and "$B_{as\text{-}received}$" are displayed in Figure 2 alongside pattern diffraction files for HI_3O_8 (04-011-9546), HIO_3 (04-010- 6560), and I_2O_5 (04-007-1333).

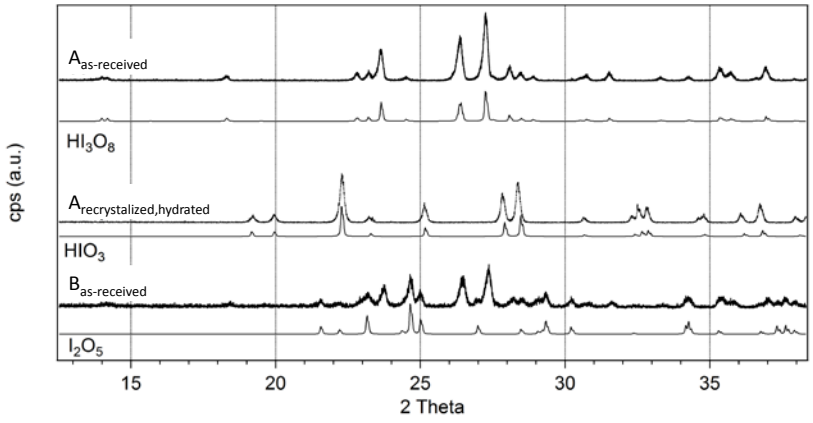

Figure 2. Powder X-ray patterns of various samples of iodine (V) oxide compared to pattern diffraction files: Sample "A" as received *vs*. # 04-011-9546; "$A_{recrystalized,hydrated}$" which is fully hydrated and recrystallized "A" *vs*. # 04-010-6560; and "B" as received sputtered coated with Au/Pd. *vs.* # 04-007-1333.

Consistent with the DSC/TGA results, the diffractogram for sample as received sample "A" closely matches the calculated profile for HI_3O_8, a monoclinic crystal with a $P2_{1/n}$ space group. Lattice constants for sample "A" were measured and refined yielding a = 7.548 Å, b = 7.687 Å, c = 11.338 Å**,** β = 90, and V = 657.8 $Å_3$ which agree well with standard values for HI_3O_8 (04-011-9546).[29] It should be noted that in 2005, Fischer concluded the molecular structure of HI_3O_8 can be thought of as an adduct of HIO_3 and I_2O_5 (*i.e.* HIO_3-I_2O_5)[28] and our results are consistent with this assertion.

The diffractogram for sample "$A_{recrystalized,hydrated}$" features none of the reflections observed in sample "A", indicating that it is a completely different substance, and is indeed a perfect match to the powder fraction file of HIO_3. This confirms the DSC/TGA results that the HI_3O_8, once pulverized and exposed to humid air above 65% RH for sufficient time, completely converts to the fully hydrated oxide, HIO_3.

The third experimental diffractogram, that of sample "B", shows the first indication of the presence of any I_2O_5. It is important to note that for this measurement, unlike the previous two, sample "B" was sputtered with a thin layer of Au/Pd in an effort to protect the oxide from hydration from water vapor in the air. This was done because these PXRD scans were measured over a period of 20 hrs, and any residual humidity would have hydrated the material. When compared to the powder diffraction file for I_2O_5 (07-007-1333), we find that a major component of the sample is indeed I_2O_5 as well as a significant amount HI_3O_8. From the strongest peaks of each diffraction pattern we estimate the abundance to be ~2:1 ratio of I_2O_5/HI_3O_8 (i.e. 65%

I_2O_5). This is somewhat less than the abundance calculated from TGA, and the discrepancy is likely due to the slow hydration of the sample during the measurement in spite of the sputter coating.

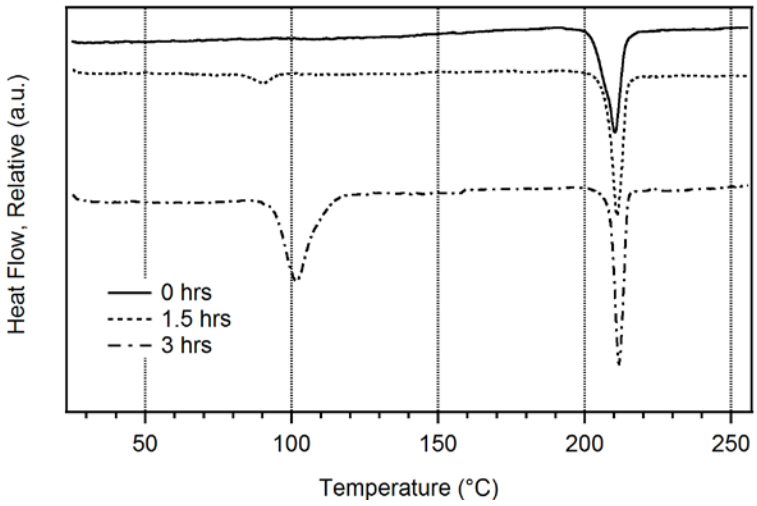

Figure 3. Heat flow thermograms obtained by differential scanning calorimeter (DSC) of samples of recrystallized HI_3O_8 that have been exposed to air at a 70% relative humidity for various amounts of time. Samples were run under air with a temperature ramp rate of 2 °C/min.

4.2. Hydration of $HI_3O_8 \rightarrow HIO_3$

To examine the hydration of $HI_3O_8 \rightarrow HIO_3$ more closely, a recrystallized sample "A" was pulverized and then exposed to air with a relative humidity of 40-72%. Samples exposed to a relative humidity < 50% were found to be stable over a period of weeks with no evidence of hydration. When the relative humidity was increased to 70 ± 2%, the samples were observed to hydrate completely to HIO_3 over a period of a few hours. Figure 3 plots the evolution of the two dehydration peaks in the calorimetric thermograms as a function of exposure to ~70% humidity. Initially absent, the peak associated with H_2O loss from HIO_3 starts to grow in at ~90 °C, and increases with intensity with humidity exposure. The peak also shifts to higher temperature, perhaps suggesting a stabilization of the HIO_3 structure with increasing fractional hydration. No significant change is observed in the second dehydration step at ~210 °C indicating the reversibility of the first hydration process.

This same process was monitored with PXRD and Figure 4 shows the change in the PXRD spectra of the same sample where the dominate diffraction peaks from both phases can be observed at 2 theta angles between 20 and 30 degrees. Interestingly, the rate of increase in HIO_3 appears to accelerate over the course of the measurement, in contrast with what was observed for

the first hydration step of $I_2O_5 \rightarrow HI_3O_8$ over time as well as a proportionate decrease in I_2O_5. The width of each peak appears to be constant indicating that the crystallinity is maintained during the hydration process.

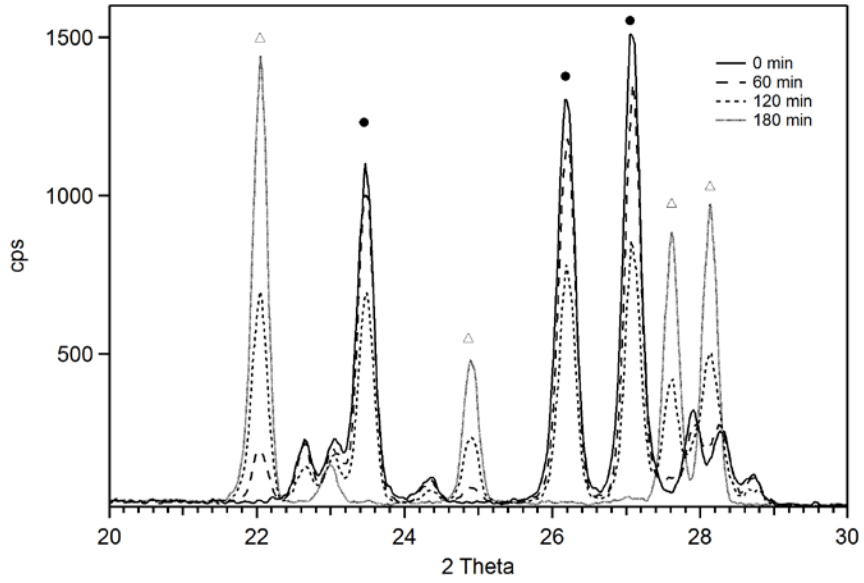

Figure 4. Powder X-ray diffraction recordings displaying the conversion of HI_3O_8 (●) → HIO_3 (Δ), sample "Arc", with increasing hydration time; open atmosphere, ~70% relative humidity

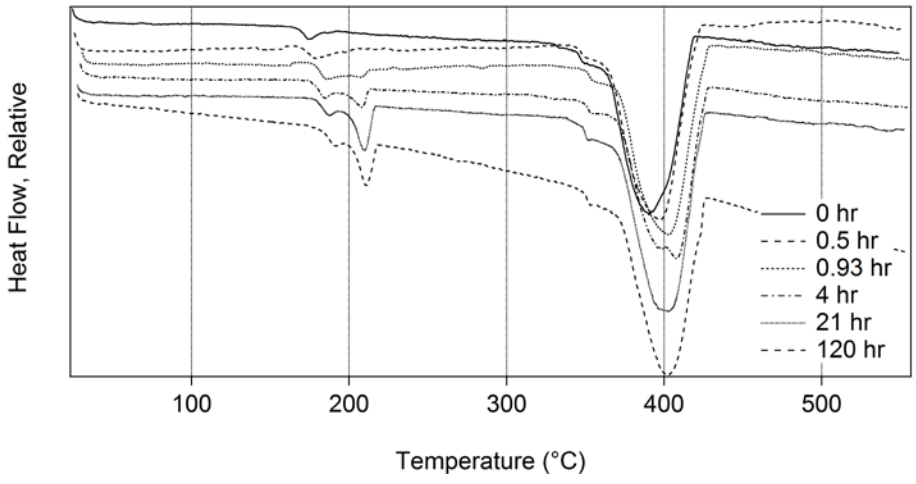

Figure 5. Evolution of the DSC thermograms of sample "$B_{as\text{-}received}$", (initially ~85% I_2O_5) during exposure to air with a 40 % relative humidity. Samples were run under air with a temperature ramp rate of 2 °C/min.

4.3. Hydration of $I_2O_5 \rightarrow HI_3O_8$

The first hydration step, that is $I_2O_5 \rightarrow HI_3O_8$, was examined in more detail by exposing sample "$B_{as\text{-}received}$" (uncoated) to air with a relative humidity of 40% over a period of several days. Samples of the exposed material were retrieved periodically and subjected to DSC/TGA analysis. Figure 5 plots the thermograms of this material after humidity exposure for 0, 0.5, 0.9, 5.0, 21, and 120 hrs. As was observed previously, the broad I_2O_5 decomposition peak appears between 360 and 420 °C, and does not change significantly upon hydration. From top to bottom, the two peaks associated with the dehydration of HI_3O_8 grow-in with increasing humidity exposure. Interestingly, the lower temperature peak at 175 °C grows in first followed by the higher temperature peak. In addition to the increase in intensity, the temperature corresponding to the minimum of each peak also increases, ultimately converging on 210 °C for the higher temperature peak, consistent with what was observed in the recrystallized HI_3O_8 spectrum. As humidity exposure is increased, mass loss (H_2O) associated with the 210 °C peak increases, however, the mass loss at 175 °C remains constant in the TGA. The reason for this effect is unclear and was not witnessed by Selte and Kjekshus,[21] though we speculate that it could be due to an amorphous form of HI_3O_8 formed on the surface of the particles. No peaks were observe ~ 100 °C (not shown) indicating that only the first hydration step is occurring over this time scale and humidity of this experiment.

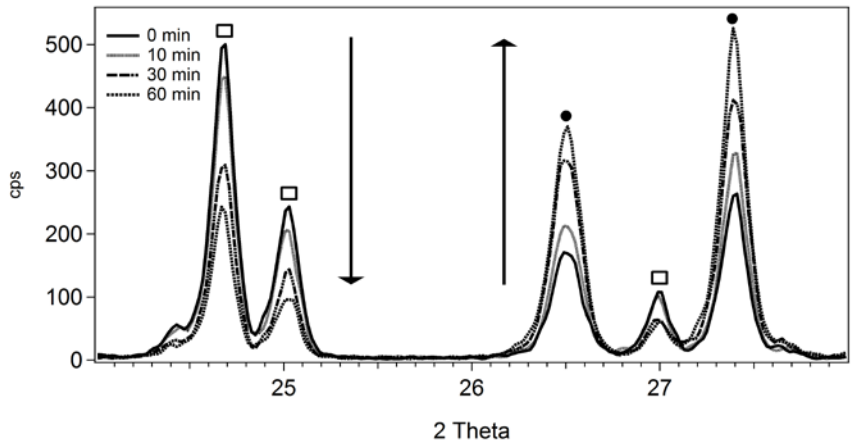

Figure 6. Powder X-ray diffraction recordings displaying the conversion of I_2O_5 (□) → HI_3O_8 (●), sample "B", with increasing hydration time; open atmosphere, ~40% relative humidity.

Another noteworthy feature in these thermograms is the width of the ~ 200 °C peak is significantly broader than those observed in the recrystallized sample shown in Figure 1. A careful comparison of the diffractograms of "$A_{recrystalized}$" to that of the humidity hydrated "B," however, showed no indication of additional broadening or shifting of the various diffraction peaks, suggesting that the broadening in the thermograms is probably not due to presence of amorphous material in the interior of the particles. The source of the structure remains unknown

and may be examined more closely in later studies. It is important to emphasize that the mass loss in the TGA upon dehydration, in spite of this unknown complexity, is still a valid indicator of the amount of hydrate present in the material and can still be used as a quantitative measure of the hydration rate.

The first hydration step was also monitored by PXRD where the dominate diffraction peaks for I_2O_5 and HI_3O_8 phases can be observed at 2 theta angles between 24 and 28 degrees. Figure 6 displays this region of the diffractogram for sample "B" (uncoated) at various times while exposed to an open atmosphere at a relative humidity of 40%. Clearly observed is a monotonic increase of HI_3O_8 over time as well as a proportionate decrease in I_2O_5. The width of each peak appears to be constant indicating that the degree of crystallization is maintained during the hydration process.

5. DISCUSSION

We begin the discussion by comparing the hydration rates of the first and second hydration steps of I_2O_5. Figure 7 summarizes the hydration progress as monitored by XRD in the data presented in Figure 4 and 6 as well as the rates of hydration with DSC-TGA of sample "B". The hydration of I_2O_5 into HI_3O_8 appears to occur in two phases: an initial phase occurs at a constant rate of 0.73 %·min^{-1} followed by a slower, approximately linear rate after ~70% conversion at about 0.023 %·min^{-1}. This second phase suggest the onset of a rate limiting hydration mechanism. The hydration behavior of HI_3O_8 into HIO_3 appears to occur by a different mechanism, exhibiting a delay followed by an accelerating rate of conversion until completion.

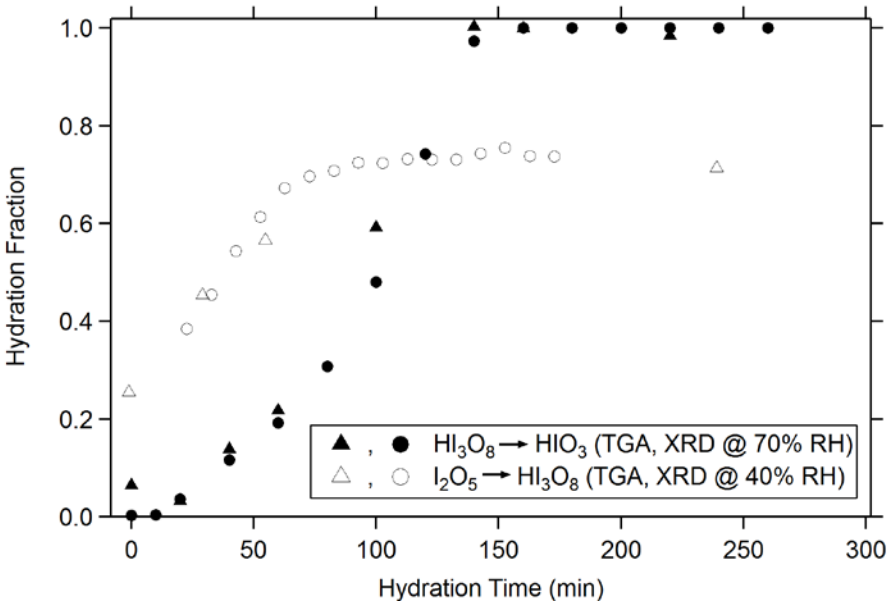

Figure 7. Degree of hydration over time as various samples are exposed to air with a relative humidity of 40% (I_2O_5) or 70% (HI_3O_8). The composition was measured via XRD (circle markers) and TGA (triangle markers).

To further investigate the two hydration mechanisms of I_2O_5, the conversion rates of coated samples were measured as a function of the thickness of a Au/Pd layer, sputtered upon the powder. Figure 8 depicts hydration curves for select specimens that were uncoated or coated with a layer of Au/Pd. As one would expect, all samples coated with Au/Pd possessed rates of formation for HI_3O_8 less than that of an uncoated specimen. A factor greater than 8 is observed for the initial rate of hydration (k_1) for the uncoated specimens versus the coated specimens (0.67 % min^{-1} & 0.08 % min^{-1}), see Table 2. Interestingly, the second rate of hydration (k_2) does not appear to differ significantly between the coated and uncoated samples, 0.0170% min^{-1} and 0.0165 % min^{-1}, respectively. Furthermore, the ratio of hydration between step 1 and 2, (k_1/k_2), is ~39 for the uncoated particles versus ~5 for the coated particles. This observation will be discussed further later in the text.

Models used to describe solid state reactions with a decreasing rate with a clear reaction progression, like this system, are termed decelerating models.[34] These models are typically utilized to described nucleation or nuclei growth in terms of physical parameters such as: surface area, volume, pressure, temperature, particle size, etc. In particular, hydration models commonly show two hydration regimes, the first assigned to nucleation and growth and the second to a diffusion limited step.[35] For the case of 3-dimensional shaped particles (i.e. spheres, cubes, and cylinders) in the presence of a reactant like water vapor, it is known that nucleation and growth begins at the particle surface and then will proceed toward the core of the particle. Initially the water vapor at or near the particle surface is able to freely penetrate through the particle at a velocity that does not limit the rate of nucleation. However, in the case of $I_2O_5 \rightarrow HI_3O_8$, as the surface and outer layers are passivated by the formation of the hydrate material (HI_3O_8) the diffusion of water vapor becomes limited. This process can also be described by a shrinking core model where greater hydration rates are associated with decreasing particle size and higher yields of converted product before diffusion becomes limiting and the conversion rate is slowed.[36] Another name for this type of chemical reaction is topochemical. Other variables utilized to describe acceleratory processes for solid state reactions such as hydration evaluate the ratio of the rate of nucleation versus diffusion for mechanistic insight.[37,38] Large values for the rate ratio can suggest predominately lateral product (hydrate) growth at the surface (*i.e.* wetting the surface) of the particle which immediately coalescence into a passivating layer of hydrate. Smaller values suggest more spatially random nucleation sites proceeding lateraling with a faster more dominate rate of hydration that proceeds inward from the surface to the core of the particle *i.e.* diffusion. Given the previous descriptions it appears that the uncoated specimens in Figure 8 reflect an initial anisotropic growth phase followed by a less significant diffusion limited phase of hydration. However, the coated specimens in Figure 8 reflect hydration ratios of an initial nucleation phase limited due to randomly spatially located active sites which progress at a similar rate as the diffusion limited phase.

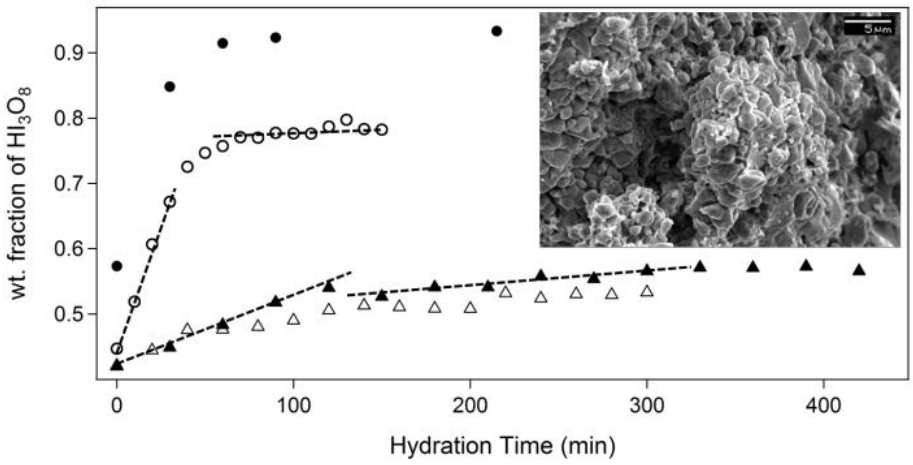

Figure 8. Plot of the weight fraction change for HI_3O_8 versus hydration time for sample "B"-I_2O_5 uncoated (circles) and coated (triangles) with Au/Pd in an open atmosphere at ~40% relative humidity measured via PXRD. Dashed lines are provided to guide the eyes to the initial rate (*k*1) and second rate (*k*2) between the two sample types. Inset: electron microscope image of the surface morphology of sample "B."

Table 2. Tabulated values for rates (*k*1 and *k*2) of conversion for $I_2O_5 \rightarrow HI_3O_8$ from Figure 8. αHI_3O_8 = weight fraction of HI_3O_8

Sample	k_1 (αHI_3O_8 min^{-1})	r^2	k_1 (αHI_3O_8 min^{-1})	r^2
? Uncoated 1	0.00568 ± 0.002	0.89	0.00011 ±3.3x10^{-5}	0.91
? Uncoated 2	0.00762 ± 0.0003	0.99	0.00023 ± 8.1x10^{-5}	0.53
? Coated 1	0.00063 ± 9.9x10^{-5}	0.89	0.00016 ± 3.3x10^{-5}	0.74
? Coated 2	0.00102 ± 3.9x10^{-5}	0.99	0.00017 ± 4.7x10^{-5}	0.74

Furthermore, the effects of coating the specimen with Au/Pd appear to have simply reduced the number of available nucleation sites on the surface of the particle thereby limiting the rate of formation of HI_3O_8. Another view of this effect is that by semi-passivating the surface of the particles only random areas of the surface, not covered by Au/Pd grains, are active to nucleate and grow; thus sputter coating the particles has artificially induced a spatially limited rate of surface nucleation. Further supporting evidence for this explanation is the fact that the uncoated specimen reaches ~75% HI_3O_8 before diffusion effects limit the rate of product formation. However, the coated specimen only reaches ~47% HI_3O_8 before diffusion dictates the rate of hydration. Ultimately, coating the particle's surface reduced the number of available nucleation sites thus decreasing the amount of HI_3O_8 formed during the nucleation and growth phase.

6. CONCLUSION

The hydration of iodine (V) oxide has been examined utilizing DSC-TGA and PXRD and confirmed to occur in two discrete steps. The first step is the hydration of I_2O_5 into HI_3O_8 which occurs at low relativity humidity (40%) and occurs on the time scale of ~100 min. The second hydration step produces a more weakly bound water molecule, as evidenced by its lower dehydration temperature, and occurs more readily in samples with a larger surface area and a relative humidity exceeding ~65%. Hydration of I_2O_5 to HI_3O_8 proceeds initially quickly via a nucleation and growth pathway followed by a diffusion limited step in the formation of HI_3O_8. Stability of I_2O_5 under ambient conditions will require some type of passivation layer else it will convert to HI_3O_8. Interestingly, it has been observed that dissolving any of the forms of iodine (V) oxides in water, upon evaporation, can produce any of the hydrated forms. This process is very sensitive to the relative humidity, particle size, and the presence of impurities in the sample. Hydration of HI_3O_8 to HIO_3 proceeds at a similar overall rate as that of the first hydration step, however the mechanistic is one that is accelerating. It appears from this work that the mechanism proceeds via an initial induction phase then accelerates exponentially to full conversion of the starting reactant (HI_3O_8). Further work will be centered on understanding this phenomenon.

It appears from this work and the literature that hydration rates are going to be dependent on the particle size, shape, available surface area and RH. Smaller particles should have higher hydration rates and particles shapes with higher surface area to volume, *e.g.* plate like crystals, should possess large hydration rates as well. The relative humidity level would be suspected to play some role in the hydration rates of this oxide, but more significant is likely the particle dimensions (surface area to volume) and we can imagine that coarser particles will be more stable than finer particles *e.g* nanoparticles. Thus a stable nanocomposite of Al/I_2O_5 under ambient conditions seems unlikely at the moment unless new passivation techniques are realized for this oxidizer in its anhydride form.

Stoichiometric balance between fuel and oxidizer for the iodine (V) oxide binary mix should be revisited knowing that the oxidizer is most probably not in its anhydride form (I_2O_5), but as HI_3O_8/HIO_3 when processed under ambient environments or stored under non-ideal conditions. Furthermore, validation of the purity of the as-delivered iodine (V) oxide compound is paramount towards understanding the initial state of the reactants within a binary mixture. For example, Scheme 2 shows the overall oxidation-reduction reaction between aluminum and the various iodine (V) oxides. For comparative purposes, enthalpy of formation for HI_3O_8 (-415.8 kJ/mol) was qualitatively calculated ΔH_f for HIO_3 were obtained from Reference 39 and ΔH_f for I_2O_5 (172.35 kJ/mol) is an average of three values from Reference 19.

Scheme 2. Enthalpy of Reaction

$$10Al(s) + 3I_2O_5(s) \rightarrow 5Al_2O_3(g) + 3I_2(g);$$

$$\Delta H_{rxn} = -6.04 \text{ kJ/g or } -25.49 \text{ kJ/cm3}, \rho gas=0.026 \text{ mol/cm}^3$$

$$10Al(s) + 2HI_3O_8(s) \rightarrow 5Al_2O_3(g) + 3I_2(g) + H_2O(g);$$

$$\Delta H_{rxn} = -5.93 \text{ kJ/g or } -25.06 \text{ kJ/cm3}, \rho gas=0.029 \text{ mol/cm}^3$$

$$10Al(s) + 6HIO_3(s) \rightarrow 5Al_2O_3(g) + 3I_2(g) + 3H_2O(g);$$

$$\Delta H_{rxn} = -5.79 \text{ kJ/g or } -23.35 \text{ kJ/cm3}, \rho gas=0.036 \text{ mol/cm}^3$$

It is important to emphasize that the enthalpy for each of these reactions is similar when the iodine (V) oxides react with aluminum, however, the number of moles of gas produced varies greatly. Given the importance that gas generation and enthalpy play on reaction rates, controlling the hydration state is critical. Furthermore, it is believed that corrosive gases (HI and I_2) and possibly hydrogen gas (H_2) are released during dehydration of the oxidizer in its hydrated or acidic forms which could affect reaction rates and maximum pressure pulses when combined with a fuel.[40] Ultimately different forms of the oxidizer could lead to variances in properties such as combustion velocity (burn rate) or sensitivity measures (ESD, impact, friction). In fact, initial studies conducted by our group have shown that during dehydration of the oxidizer when mixed with nano-aluminum that preignition occurs before decomposition of I_2O_5 near the point of dehydration.[40,41]

Acknowledgements

The authors wish to thank Prof Karen Martirosyan for preparing and donating the anhydrous I_2O_5 material used in this work. The authors would also like to acknowledge the support of Dr. Curt Johnson and Dr. Jerry Boatz for discussions of the calculation of the heat of formation for HI_3O_8. This research was performed while B.K.L and S.B.E. held National Research Council Research Associateship Awards. This work was supported by research grant 3002NW from the Air Force Office of Scientific Research and Program Officer Dr. Michael Berman. The authors would also like to acknowledge the support of Dr. Amanda M. Schrand.

References

1. Fischer, S. H. and Grubelich, M. C. A Survey of Combustible Metals, Thermites, and Intermetallics for Pyrotechnic Applications. 32nd AIAA/ASME/SAE/ASEE Joint Propulsion Conference, July **1996,** lake Buena Vista, FL

2. Martisyan, K. S.; Wang, L.; Vicent, A. and Luss, D. Nanoenergetic Gas-Generators: Design and Performance. Propellants, Explos., Pyrotech. **2009**, *34*, 532 – 538

3. Dlott, D. D. Thinking big (and small) about energetic materials. *Materials Science and Technology*, **2006**, *22*, 463-473

4. Apperson, S.; Shende, R. V.; Subramanian, S.; Tappmeyer, D.; gangopadhyay, S.; Chen, Z.; Gangopadhyay, P.; Redner, P.; Nicholich, S. and Kapoor, D. Generation of fast propagating combustion and shock waves with copper oxide/aluminum nanothermite composites. *Appl. Phys. Lett*. **2007**, *91*, 243109

5. Asay, B. W.; San, S. F.; Busse, J. R. and Oschwald, D. M. Ignition Characteristics of Metastable Intermolecular Composites *Propellants, Explos., Pyrotech*. **2004**, *29*, 216-222

6. Becker, C. R.; Apperson, S.; Morris, C. J.; Gangopadhyay, S.; Currano, L. J.; Churaman, W. A. and Stoldt, C. R. Galvanic Porous Silicon Composites for High-Velocity Nanoenergetics. Nano Lett. **2011**, 11, 803-807

7. Martirosyan, K. S.; Wang, L. and Luss, D. Tuning the Reactivity of Novel Nanoenergetic System Based on Iodine Pentoxide *Chem. Phys. Lett.* ***2009***, *483*, 107–110

8. Martirosyan, K. S. Nanoenergetic Gas-Generators: principles and applications. *J. Mater. Chem.* **2011**, *21*, 9400 9. Wu, Y. and Huang, F. A microscopic model for predicting hotspot ignition of granular energetic crystals in response to dropweight impacts. *Mechanics of Materials* **2011**, *43*, 835-852

10. Spitzer, D.; Comet, M.; Baras, C.; Pichot, V.; and Piazzon, N. Energetic nano-materials: Opportunites for enhanced performances. *J. Physics and Chemistry of Solids* **2010**, *71*, 100-108

11. Wang, L. L.; Munir, Z. A.; and Maximov, Y. M. Thermite reactions: their utilization in the synthesis and processing of materials. *J. Materials Science* **1993**, *28*, 3693-3708

12. Rossi, C.; Zhang, K.; Esteve, D.; Alphonse, P.; Tailhades, P.; and Vahlas, C. Nanoenergetic Materials for MEMS: A Review. *J. Microelectromechanical Systems* **2007**, *16*, 919-931

13. Dreizin, E. Metal-based reactive nanomaterials. *Prog. in Energy and Combustion* Sci. **2009**, *35*, 141-167

14. Siegert, B.; Comet, M.; and Spitzer, D. Safer energetic materials by a nanotechnological approach. *Nanoscale*, **2011**, *3*, 3534 - 3544

15. Martirosyan, K. S. Wang, L. and Luss, D. Development of nanoenergetic materials based on Al/I2O5 system. *NanoTech* **2010**, 137-140

16. Armstrong, R.W. and Elban, W. L. Materials science and technology aspects of energetic (explosive) materials. Materials Science and Technology **2006**, 22, 381 - 395

17. Blobaum, K. J.; Reiss, M. E.; Lawrence, J. M. P. and Weihs, T. P. Deposition and characterization of a self-propagating Cuox/Al thermite reaction in a multilayer foil geometry. *J. Appl. Phys.* **2003**, *94*, 2915-2922

18. Clark, B. R. and Pantoya, M. L. The aluminum and iodine pentoxide reaction for the destruction of spore forming bacteria. *Phys. Chem. Chem. Phys.* **2010**, *12*, 12653-12657

19. Chase, M. W. NIST-JANAF Thermochemical Tables for the Iodine Oxides. *J. Phys. Chem. Ref. Data.* **1996**, 25, 1297 - 1340

20. Drátovský, M. and Pačesová, L. New Information about Oxygen-containing Compounds of Iodine. *Russ. Chem. Rev.* **1968**, *37*, 243-254

21. Selte, K. and Kjekshus, A. Iodine Oxides Part II. On the System H_2O-I_2O_5. *Acta. Chem. Scand.* **1968, *22,*** 3309-3320

22. Ellestad, O. H.; Woldbaek, T.; Kjekshus, P.; Klaeboe, P. and Selte, K. Infrared and Raman Studies of Crystalline I_2O_5, $(IO)_2SO_4$, $(IO)_2SeO_4$, and I_2O_4. *Acta. Chem. Scand. A* **1981**, 35, 155- 164

23. Sherwood, P. M. A. and Turner, J. J. Mass Spectrum of iodine pentoxide and a novel reaction with copper. *J. Chem. Soc. A.* **1970**, 2349-2350

24. Sherwood, P. M. A. X-Ray Photoelectron Spectroscopic Studies of Some Iodine Compounds. **1975,** 1805-1820

25. Saunders, W. S. and Plane, M. C. Formation Pathways and Composition of Iodine Oxide Ultra-Fine Particles. *Environ. Chem.* **2005**, *2*, 299-303

26. Sherwood, P. M. A. and Turner, J. J. Vibrational spectra of compounds in the iodine pentoxide-water system and sodium iodate. *Spectrochima Acta, Part A, Molecular Spectroscopy* **1970,** *26,* 1975-1992

27. Wu, Z.; Kalia, R. K.; Nakano, A.; Vashishta, P. First-principles calculations of the structural and dynamic properties, and the equation of state of crystalline iodine oxides I_2O_4, I_2O_5, and I_2O_6. *J. Chem. Phys.* **2011**, *134*, 204501-204514

28. Fischer A. Redetermination of HI_3O_8, an adduct of formula $HIO_3 \cdot I_2O_5$. *Acta Cryst.* **2005**, *E61*, i278-i279

29. Bahl, R. K. and Partington, J. R. Lower oxides and sulphates of iodine. *J. Chem. Soc.* **1935**, 1258-1263

30. Daehlie, G. and Kjekshus, A. Iodine Oxides Part 1. On I_2O_3- SO_3, I_2O_3-$4SO_3$-H_2O, I_2O_3-SeO_3 and I_2O_4. Acta. Chem. Scand. **1964**, *18*, 144

31. Kumar, R.; Saunders, R. W.; Mahajan, A. S.; Plane, J. M.; Murray, B. Physical properties of iodate solutions and the deliquescence of crystalline I_2O_5 and HIO_3. *J. Atmos. Chem. Phys.* **2010**, *10*, 12251-12260

32. Selte, K. and Kjekshus, A. Iodine Oxides Part III. The Crystal Structure of I_2O_5. *Acta. Chem. Scand.* **1970, *24,*** 1912-1924

33. Stahl, K. and Szafranski, M. A Single-Crystal Neutron Diffraction Study of HIO_3 @ 295 and 30 K and of DIO_3 at 295 K Acta Chem. Scand. **1992**, 46, 1146-1148

34. Khawam, A. and Flnagan, D. R. Solid-State Kinetic Models: Basics and Mathematical Fundamentals. *J. Phys. Chem. B.* **2006**, *110*, 17315-17328

35. Peterson, V. K.; Neuman, D. A. and Livingston, R. A. Hydration of Tricalcium and Dicalcium Silicate Mixtures Studied Using Quasielastic neutron Scattering. *J. Phys. Chem. B.* **2005**, *109*, 14449-14453

36. Allen, A. J.; McLaughlin, J. C.; and Neumann, D. A. In situ quasi-elastic scattering characterization of particle size effects on the hydration of tricalcium silicate. *J. Mater. Res.* **2004**, *19*, 3242- 3254

37. Peterson, V. K. and Whitten, A. E. Hydration Processes in Tricalcium Silicate: Application of the Boundary Nucleation Model to Quasielastic Neutron Scattering Data. *J. Phys. Chem. C.*, **2009**, 113, 6, 2347-2351

38. Scherer, G. W.; Zhang, J.; and Thomas, J. J. Nucleation and Growth Models for Hydration of Cement *Cement and Concrete Research* 42, **2012**, 982-993

39. Lide, D. R. CRC Handbook of Chemistry and Physics, 86th edition, **2005-2006**, section 5-13

40. B.K. Little, E.K. Avjian, M. Bogle, Nittinger, J. C., S.B. Emery, A. Schrand, and C.M. Lindsay. *Trade-Off Between Sensitivity and Performance in nano-Aluminum/Iodine (V) Oxide*. Proceedings of the Joint Army Navy NASA Air Force, 38th Propellant and Explosives Development and Characterization Meeting, Dec 4, **2012**b

41. Little, B. K.; Welle, E. W.; Emery, S. B.; Bogle, M. B.; Ashley, V. L.; Schrand, A.; and Lindsay, C. M. *Chemical Dynamics of Nano-Aluminum/Iodine (V) oxide*. Proceedings of the Joint APSSCCM/ AIRAPT Conference, Seattle WA, **2012**

DISTRIBUTION LIST
AFRL-RW-EG-TR-2014-135

*Defense Technical Info Center
8725 John J. Kingman Rd Ste 0944
Fort Belvoir VA 22060-6218

AFRL/RWME (1)
AFRL/RWOC-1 (STINFO Office)